




# Three-dimensional radial echo-planar spectroscopic imaging for hyperpolarized $^{13}\text{C}$ MRSI in vivo

Marcel Awenius<sup>1,2,3</sup>  | Helen Abeln<sup>1,3,4</sup> | Melanie Müller<sup>1</sup> | Vanessa L. Franke<sup>1</sup>  | Gino Rincon<sup>1,2,5</sup> | Christin Glowa<sup>6,7,8</sup> | Michaela Schmitt<sup>6,8,9</sup> | Renate Bangert<sup>1</sup> | Dominik Ludwig<sup>1</sup> | Andreas B. Schmidt<sup>10,11</sup> | Tristan A. Kuder<sup>1</sup> | Mark E. Ladd<sup>1,2,12</sup> | Peter Bachert<sup>1,2</sup> | Philipp Biegger<sup>1</sup> | Andreas Korzowski<sup>1,5</sup> 

## Correspondence

Andreas Korzowski, German Cancer Research Center (DKFZ), Division of Medical Physics in Radiology, Im Neuenheimer Feld 223, 69120 Heidelberg, Germany.

Email: [a.korzowski@dkfz.de](mailto:a.korzowski@dkfz.de)

## Funding information

German Cancer Consortium

## Abstract

**Purpose:** To demonstrate the feasibility of 3D echo-planar spectroscopic imaging (EPSI) technique with rapid volumetric radial k-space sampling for hyperpolarized (HP)  $^{13}\text{C}$  magnetic resonance spectroscopic imaging (MRSI) in vivo.

**Methods:** A radial EPSI (rEPSI) was implemented on a 3 T clinical PET/MR system. To enable volumetric coverage, the sinusoidal shaped readout gradients per k-t-spoke were rotated along the three spatial dimensions in a golden-angle like manner. A distance-weighted, density-compensated gridding reconstruction was used, also in cases with undersampling of spokes in k-space. Measurements without and with HP  $^{13}\text{C}$ -labeled substances were performed in phantoms and rats using a double-resonant  $^{13}\text{C}/^1\text{H}$  volume resonator with 72 mm inner diameter.

**Results:** Phantom measurements demonstrated the feasibility of the implemented rEPSI sequence, as well as the robustness to undersampling in k-space up to a factor of 5 without advanced reconstruction techniques. Applied to measurements with HP  $[1-^{13}\text{C}]\text{pyruvate}$  in a tumor-bearing rat, we obtained well-resolved MRSI datasets with a large matrix size of  $12^3$  voxels covering the whole imaging FOV of  $(180\text{ mm})^3$  within 6.3 s, enabling to observe metabolism in dynamic acquisitions.

**Conclusion:** After further optimization, the proposed rEPSI method may be useful in applications of HP  $^{13}\text{C}$ -tracers where unknown or varying metabolite resonances are expected, and the acquisition of dynamic, volumetric MRSI datasets with an adequate temporal resolution is a challenge.

## KEYWORDS

$^{13}\text{C}$  MRSI, dynamic nuclear polarization, echo-planar, hyperpolarization, radial

For affiliations refer to page 40

This is an open access article under the terms of the [Creative Commons Attribution-NonCommercial](https://creativecommons.org/licenses/by-nc/4.0/) License, which permits use, distribution and reproduction in any medium, provided the original work is properly cited and is not used for commercial purposes.

© 2024 The Author(s). *Magnetic Resonance in Medicine* published by Wiley Periodicals LLC on behalf of International Society for Magnetic Resonance in Medicine.

## 1 | INTRODUCTION

Hyperpolarized (HP)  $^{13}\text{C}$  MRI is an emerging molecular imaging technique with enormous clinical potential,<sup>1</sup> because it enables to monitor the distribution of  $^{13}\text{C}$ -labeled metabolites in vivo as well as their metabolic turnover in quasi real time. However, the rapid decay of the non-recoverable HP state through  $T_1$  relaxation and metabolic conversion demands fast imaging sequences.<sup>2,3</sup> To achieve the often required high spatiotemporal resolution, metabolite-specific imaging techniques are typically used, for example, EPI<sup>4,5</sup> with spectral-spatial RF pulses or spectrally selective balanced SSFP (bSSFP).<sup>6–9</sup> These approaches rely on the fact that the detectable  $^{13}\text{C}$  signals in vivo originate from only a sparse number of metabolites with well-defined chemical shifts (mostly focused on pyruvate and lactate).

However, there are applications where metabolite-specific approaches face challenges or the acquisition of the complete spectral information is desired. Such applications include (1) situations with unknown metabolic conversions (i.e., it remains unclear what signals will be expected); (2) the chemical shifts are varying (e.g., pH-based biosensors like zymonic acid [ZA]<sup>10</sup> or Z-OMPD<sup>11</sup>); or (3) the spectral pattern is known, but too complex to be captured efficiently by metabolite-specific imaging (e.g.,  $[1,2-^{13}\text{C}]$ pyruvate<sup>12</sup>). In these cases, spectroscopic imaging (SI) techniques are recommended, but the long signal acquisition window to obtain the desired well-resolved spectral information makes SI acquisitions intrinsically slow. Even accelerated SI techniques like echo-planar spectroscopic imaging (EPSI)<sup>13,14</sup> are still substantially slower than metabolite-specific imaging approaches. To further improve the temporal resolution for rapid magnetic resonance spectroscopic imaging (MRSI) of HP  $^{13}\text{C}$ , more efficient sampling of k-space is crucial, either using special gradient trajectories or performing undersampling. In this regard, radial k-space sampling is well-suited as it is robust against undersampling and potentially allows for further acceleration by the means of compressed-sensing techniques.<sup>15</sup> Recently, a 2D radial EPSI (rEPSI) technique for HP  $^{13}\text{C}$  MRSI was proposed.<sup>16</sup> An extension of such a strategy for whole-volume coverage has been demonstrated for X-nuclei MRSI,<sup>17</sup> but not yet attempted for HP  $^{13}\text{C}$ .

The purpose of this study is to demonstrate the feasibility of a 3D EPSI technique with volumetric radial k-space sampling for HP  $^{13}\text{C}$  MRSI in vivo. The successful implementation of a rEPSI sequence, its performance in metabolic phantom measurements and in small-animal experiments after injection of HP  $[1-^{13}\text{C}]$ pyruvate will be presented, as well as the offered possibilities on further improving the temporal resolution.

## 2 | METHODS

### 2.1 | Three-dimensional rEPSI

Figure 1 illustrates the implemented rEPSI approach. For simultaneous sampling of the spatial and temporal dimension, a sinusoidal-shaped, oscillating readout gradient was applied, constituting a single spoke in k-t-space. To cover the 3D k-space in a radial manner, the scheme described in Figure 1 is executed multiple times while rotating the readout gradient direction according to the following formulas:

$$\varphi(i) = 2\pi \bmod\left(\frac{i}{\alpha}, 1\right), \quad (1)$$

$$\theta(i) = \text{acos}\left(\frac{i}{M}\right), \quad (2)$$

with  $\varphi(i)$  being the polar and  $\theta(i)$  the azimuthal angles for spoke  $i$ ,  $\alpha$  is the golden ratio and  $M$  the total number of spokes.  $M$  is defined by the rounded-up resolution  $R$  as a number of isotropically acquired voxels via the Nyquist criterion:

$$M = 2\pi\left(\frac{R}{2}\right)^2. \quad (3)$$

Using this sampling strategy, the spatial resolution is defined by the number of points sampled within a gradient lobe. As data reconstruction is performed by separating odd and even echo data (as described below), the acquired spectral bandwidth is given by the time difference of gradient lobes with same polarity ( $t_d$  in Figure 1), whereas the spectral resolution is given by the number of echoes of same polarity that are acquired within a single excitation.

Because this sampling strategy enables whole-volume acquisitions, a short, rectangular-shaped RF pulse of 200  $\mu\text{s}$  was applied for excitation without slice-selection gradients. Note that each full-radial spoke is preceded by a prephasing gradient to ensure continuous sampling in one direction of k-space from  $k_{\text{max}}$  to  $-k_{\text{max}}$ , and vice versa.

### 2.2 | Data reconstruction and processing

Data reconstruction and processing was performed with custom-written scripts in MATLAB R2019b (The MathWorks).

Reconstruction of  $^{13}\text{C}$  raw data started by sorting data from odd and even echoes individually into corresponding k-t-space matrices. A gridding reconstruction<sup>18</sup> was applied that distributes the expected, radially sampled data points onto a Cartesian grid in a distance-weighted manner, compensating for variable k-space sampling density. Here, onefold zero-filling in spatial and in temporal

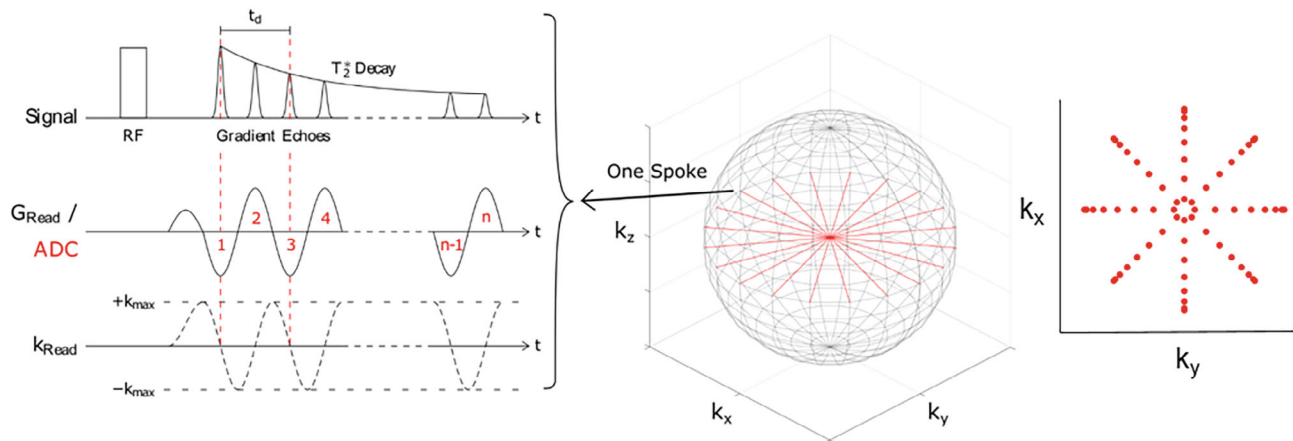


**FIGURE 1** Sequence diagram of the implemented 3D radial echo-planar spectroscopic imaging. After a rectangular whole-volume RF excitation pulse and a prephaser gradient, an oscillating sinusoidal readout gradient  $G_{\text{Read}}$  with  $n$  lobes is applied. After each full-radial spoke (sampling both sides from  $k$ -space center), the gradient direction is rotated around the center of the sphere to radially sample  $k$ -space in all three dimensions. Note that the  $k$ -space center is traversed in the middle of each spoke. A projection of the  $k$ -space sampling density for the  $k_x$ - $k_y$  plane is displayed on the right.

domain was applied. To increase the SNR by a factor of  $\sqrt{2}$ , odd and even echoes were recombined by adding both datasets in image space after zero-order phase-correction in each voxel. Note that no further processing had been applied, that is, trajectory corrections related to gradient nonlinearities.

The post-processed  $^{13}\text{C}$  MRSI datasets were quantified using a customized implementation<sup>19</sup> of the advanced method for accurate, robust and efficient spectral fitting (AMARES) algorithm<sup>20</sup> with a Gaussian lineshape model. The quantified metabolite amplitudes were used to generate metabolite maps for overlays with morphological  $^1\text{H}$  images.

## 2.3 | Experimental setup

All measurements were performed on a 3 T clinical PET/MR system (Biograph mMR, Siemens Healthineers) with a gradient strength of 24 mT/m and a maximal slew rate of 180 T/m/s, both per axis, using a double-resonant  $^{13}\text{C}/^1\text{H}$  volume resonator with 72 mm inner diameter (Rapid Biomedical). The in vivo measurements on male tumor-bearing Copenhagen rats (syngeneic Dunning prostate adenocarcinoma R3327-HI, right hind leg) were approved by the local authorities (ref. no. 35-9185.81/G197/17) and animals were kept under standard laboratory conditions. For the hyperpolarization of  $[1\text{-}^{13}\text{C}]\text{pyruvate}$ , a SPINlab polarizer (General Electric Healthcare) was used, using a mixture of  $[1\text{-}^{13}\text{C}]\text{pyruvic acid}$  and AH111501. For the four-chamber phantom experiment, a 0.8 mL dose was applied. For the animal

experiment, a 1.5 mL dose additionally containing 0.9% sodium chloride was injected.

Calibration procedures for  $^{13}\text{C}$  reference frequencies and transmit gain on a small  $[^{13}\text{C}]\text{urea}$  phantom (integrated in an animal positioning setup) preceded all HP  $^{13}\text{C}$  MR measurements.

### 2.3.1 | Phantom measurements

As proof-of-concept, a 50-mL tube was filled with ethylene glycol (EG) ( $^{13}\text{C}$  in natural abundance) and measured with the implemented rEPSI sequence. To investigate the effects of undersampling, the EG phantom was measured with decreasing percentage of spokes to fulfill the Nyquist criterion from 100% down to 5% in individual measurements, qualitatively comparing the  $^{13}\text{C}$  intensity maps and spectra, successively. The sequence parameters were the following: matrix size =  $16^3$ , FOV =  $(200\text{ mm})^3$ , spatial resolution =  $(12.5\text{ mm})^3$ , TR = 130 ms, total acquisition time ( $T_{\text{tot}}$ ) = 53 s, spectral bandwidth = 1 kHz, echoes = 128 (each, for odd and even), flip angle =  $60^\circ$ . A total of 403 spokes were necessary to fulfill the Nyquist criterion for these adjustments.

### 2.3.2 | Four-chamber phantom

For the enzymatic phantom measurement, a four-chamber phantom was used, consisting of an outer 50-mL tube filled with water and four 1.5-mL tubes inside. Three small tubes were filled with deionized water, a thermally polarized  $[^{13}\text{C}]\text{urea}$  solution and a HP  $[1\text{-}^{13}\text{C}]\text{pyruvate}$

solution, respectively, whereas the fourth one contained lactate dehydrogenase (LDH) mixed with  $\beta$ -Nicotinamide adenine dinucleotide (reduced) and was attached to a puncture site in the cap through which a syringe could inject HP  $[1\text{-}^{13}\text{C}]$ pyruvate. The  $[^{13}\text{C}]$ urea sample consisted of a 10 M solution with 0.6% Magnevist (Bayer HealthCare).

The four-chamber phantom measurement started directly after injection of the HP  $[1\text{-}^{13}\text{C}]$ pyruvate into the upper LDH-containing tube. Time from dissolution to start of the rEPSI measurement was 44 s. The sequence parameters were the following: matrix size =  $16^3$ , FOV =  $(200\text{ mm})^3$ , spatial resolution =  $(12.5\text{ mm})^3$ , TR = 520 ms,  $T_{\text{tot}} = 52\text{ s}$ , spectral bandwidth = 1 kHz, echoes = 512 (each, for odd and even), flip angle =  $3^\circ$ . A total of 403 spokes were necessary to fulfill the Nyquist criterion for those adjustments, whereas 101 were actually acquired (undersampling factor of 4).

### 2.3.3 | In vivo measurements

For the in vivo measurement, the rEPSI scheme was executed eight times consecutively to capture the metabolism dynamically, resulting in a total measurement time of  $6.3\text{ s} \times 8 = 50.4\text{ s}$ . Time from dissolution to start of the measurement was 34 s. The sequence parameters were the following: matrix size =  $12^3$ , FOV =  $(180\text{ mm})^3$ , spatial resolution =  $(15\text{ mm})^3$ , TR = 105 ms,  $T_{\text{tot}} = 6.3\text{ s}$ , spectral bandwidth = 1 kHz, echoes = 64 (each, for odd and even), flip angle =  $3^\circ$ . A total of 227 spokes were necessary to fulfill the Nyquist criterion for those adjustments, whereas 60 were actually acquired (undersampling factor of 4). The noise level was determined from the last 5% of data points in time domain of the last dynamic dataset.

## 3 | RESULTS

### 3.1 | Phantom measurements

The feasibility of the implemented  $^{13}\text{C}$  rEPSI approach could be demonstrated in the measurements on the thermally polarized EG phantom. Figure 2 displays representative metabolite maps and localized spectra for sampling according to the Nyquist theorem (100%), as well as for undersampling. In the undersampled cases (i.e., 5% and 20% of spokes required to fulfill the Nyquist criterion), it can be seen that the structured noise because of aliasing increases when the number of spokes is reduced. From a qualitative analysis, the intensity of the aliasing artifacts was smaller than or comparable to the noise level, and therefore, rendered negligible, for an undersampling

factor of up to 5. Therefore, only  $\sim 25\%$  of the spokes, according to the Nyquist criterion, was acquired in the following measurements (undersampling factor of 4) to reduce the measurement time per time frame.

### 3.2 | Four-chamber phantom

The application of rEPSI to a  $^{13}\text{C}$  hyperpolarization experiment is shown in Figure 3, where the metabolic intensity maps of the four-chamber phantom for a single timepoint are overlaid onto a  $^1\text{H}$  gradient echo image. In addition, representative spectra from two voxels with well-resolved resonances and their fitted signals are shown. All expected resonances (i.e.,  $[1\text{-}^{13}\text{C}]$ pyruvate,  $[1\text{-}^{13}\text{C}]$ lactate, and  $[^{13}\text{C}]$ urea) are localized within the corresponding tubes, demonstrating the feasibility of the implemented rEPSI for various resonances of HP substrates and also in the context of metabolic conversion.

### 3.3 | In vivo measurement

In Figure 4, the  $^{13}\text{C}$  intensity maps of  $[1\text{-}^{13}\text{C}]$ pyruvate,  $[1\text{-}^{13}\text{C}]$ lactate, and  $[1\text{-}^{13}\text{C}]$ alanine from a representative measurement of a tumor-bearing rat can be seen, which were acquired within 6.3 s (second timepoint of the dynamic series). Representative spectra of three voxels are shown: one within the abdomen, one within the tumor-bearing leg, and one within the healthy contralateral leg as comparison. As expected, the voxel within the tumor shows an increased lactate-to-pyruvate ratio compared to the muscle voxel from the contralateral side.

Finally, the capability of the rEPSI sequence to obtain multiple timepoints for the quantification of dynamic processes was demonstrated. Figure 5 shows the quantified amplitudes of  $[1\text{-}^{13}\text{C}]$ pyruvate,  $[1\text{-}^{13}\text{C}]$ lactate, and  $[1\text{-}^{13}\text{C}]$ alanine across the dynamic series with a temporal resolution of 6.3 s. For  $[1\text{-}^{13}\text{C}]$ pyruvate, an exponential decay can be observed until  $\sim 32\text{ s}$  after start of the measurement.  $[1\text{-}^{13}\text{C}]$ lactate and  $[1\text{-}^{13}\text{C}]$ alanine show a signal build-up followed by a decay for  $\sim 25\text{ s}$  before the signal reaches the noise level. Dynamic data from four additional in vivo measurements acquired with identical experimental setup and sequence parameters are presented in Figure S1.

## 4 | DISCUSSION

In this study, we demonstrated the feasibility of a radial EPSI sequence for time-resolved, volumetric spectroscopic imaging of HP  $^{13}\text{C}$ -substances. As was shown in phantoms,

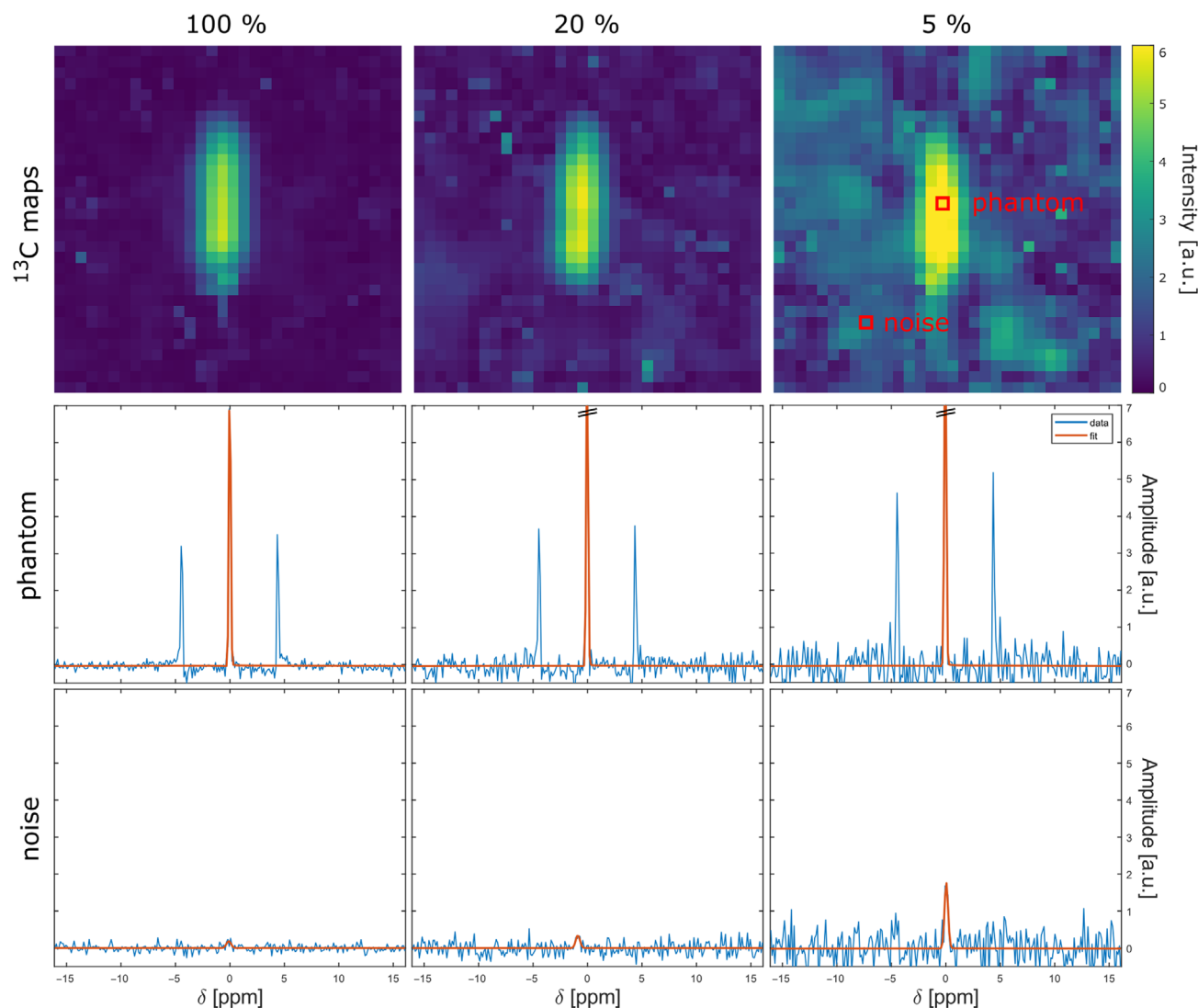


**FIGURE 2**  $^{13}\text{C}$  ethylene glycol (EG) intensity maps of a representative coronal slice (top row) for decreasing spoke sampling percentage from left to right (100%, 20%, and 5%). The voxel size after zero-filling is  $(6.23 \text{ mm})^3$ . The intensity is determined by the fitted amplitude of the center peak of EG. Spectra of the indicated representative voxel within the phantom (middle row) and in the noise region (bottom row) are shown. Note that structured noise due to aliasing increases with a higher undersampling factor. Furthermore, note that the SNR decreases with a reduced number of spokes because of less accumulated MR signal, and hence, the amplitudes are divided by the number of spokes to achieve comparable maps and spectra.

reconstruction of this radial k-space data is robust for spatial undersampling to a certain degree without introduction of severe spatial aliasing artifacts. Applying such an accelerated approach to the imaging of HP  $[1\text{-}^{13}\text{C}]$ pyruvate in vivo, MRSI datasets with large spatial matrix size of  $12^3$  and adequate differentiation between metabolites (spectral resolution of  $\sim 16 \text{ Hz}$ ) could be obtained in  $\sim 6 \text{ s}$ , enabling to capture the dynamics of metabolism. However, spatial resolution in vivo was harshly restricted to  $(15 \text{ mm})^3$  at a covered spectral bandwidth of  $1 \text{ kHz}$  because of the limitations of the gradient system. In this regard, the sinusoidal readout gradients helped lowering the demands on the hardware.

Key for the improved time efficiency in data sampling was the radial sampling of the 3D k-space by means of radial k-t-spokes. For an imaging matrix with  $12^3$  voxels, 227 spokes had to be acquired to fulfill the Nyquist condition according to Eq. (3). This is far less than the  $12^3 = 1728$  k-space encoding steps required for conventional chemical shift imaging, but a factor of  $\sim 1.57$  higher than the  $12^2 = 144$  Cartesian k-t-spokes for conventional EPSI. This factor can easily be compensated by reducing the number of sampled spokes, as was shown on a thermally polarized EG phantom where undersampling up to a factor of 5 revealed no excess aliasing artifacts compared to noise level (Figure 2). This was further



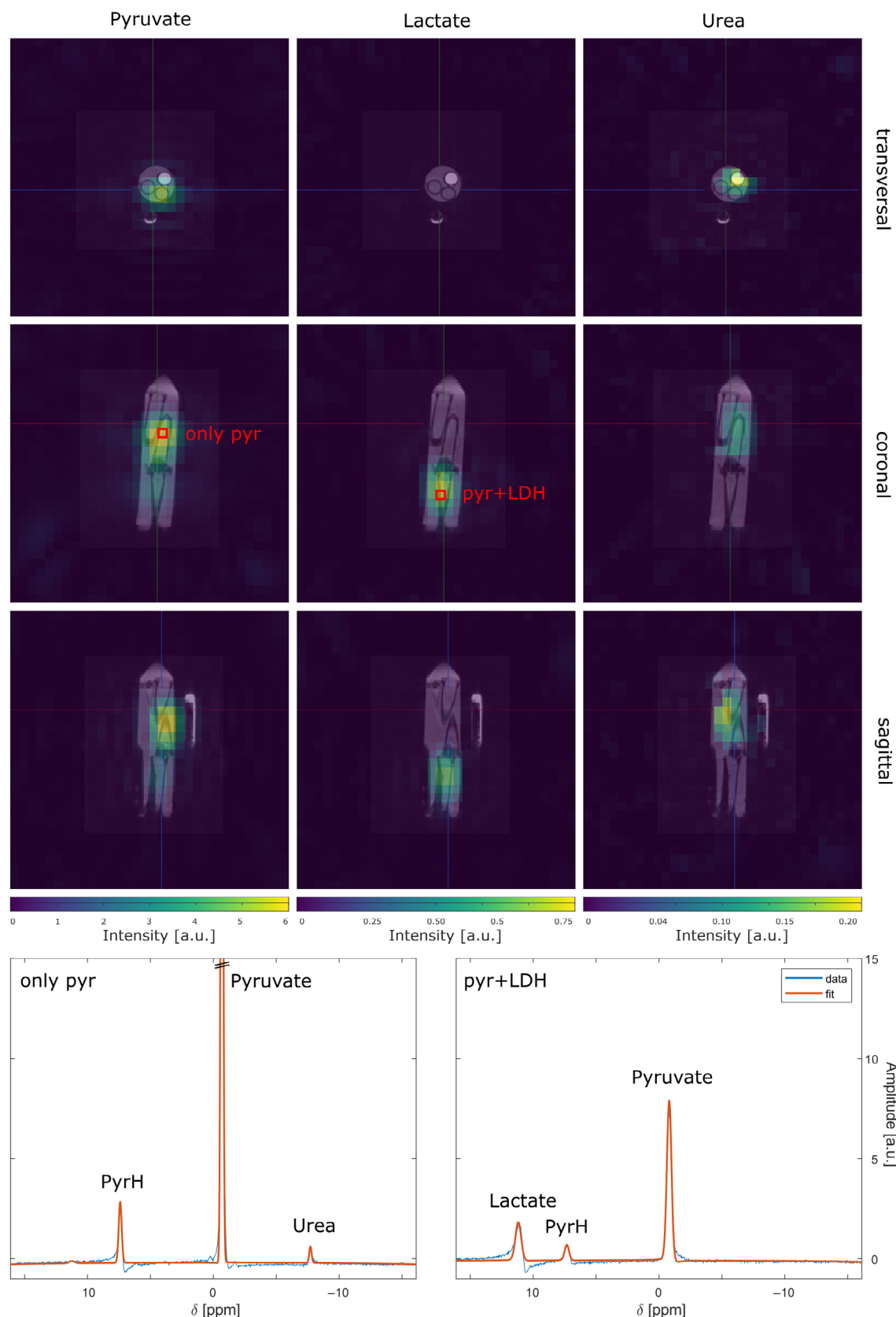


**FIGURE 3**  $^{13}\text{C}$  intensity maps of  $[1-^{13}\text{C}]$ pyruvate,  $[1-^{13}\text{C}]$ lactate, and  $[^{13}\text{C}]$ urea from the four-chamber phantom acquired with the 3D radial echo-planar spectroscopic imaging (REPSI) within 52 s (single-timeframe) and an undersampling factor of 4. Spectra of two representative voxels are shown: One within the pyruvate sample and one within the pyruvate + lactate dehydrogenase (LDH) sample. The broad point-spread function leads to voxel bleeding to neighboring voxels.

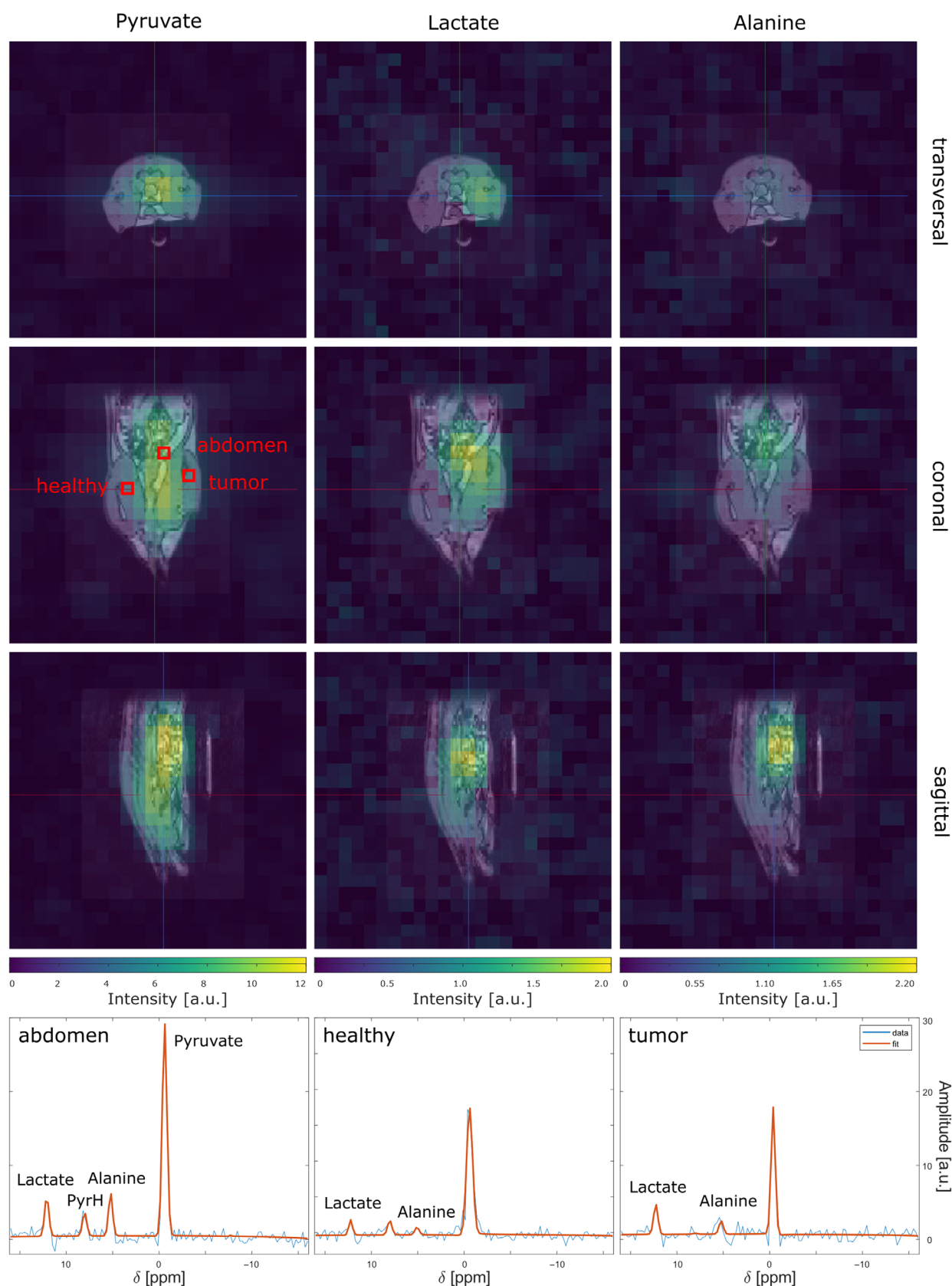


**FIGURE 4**  $^{13}\text{C}$  intensity maps of  $[1-^{13}\text{C}]$ pyruvate,  $[1-^{13}\text{C}]$ lactate, and  $[1-^{13}\text{C}]$ alanine from an in vivo measurement of a tumor-bearing rat acquired within 6.3 s (only one timeframe shown). Representative spectra of three voxels are displayed: one within the abdomen, one within the leg with implanted tumor, and one within the contralateral healthy leg for comparison.

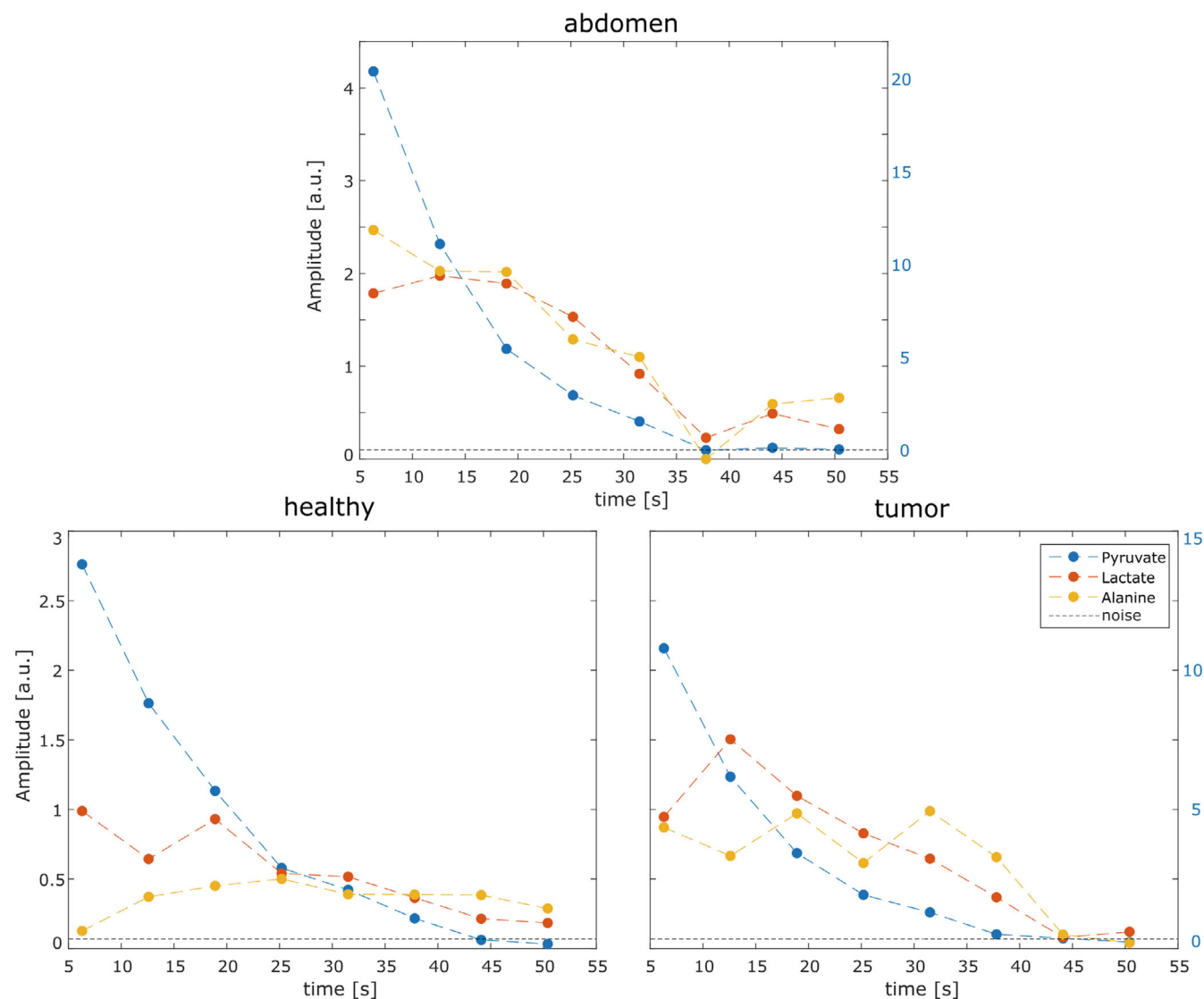


**FIGURE 5** Quantified amplitudes of  $[1-^{13}\text{C}]$ pyruvate (blue),  $[1-^{13}\text{C}]$ lactate (red), and  $[1-^{13}\text{C}]$ alanine (yellow) from the dynamic scan with eight timepoints and a temporal resolution of 6.3 s. The scale for pyruvate was divided by five and is displayed on the right axes of the plot. The data shows the three selected voxels of Figure 4, one within the abdomen, one within the leg with implanted tumor, and one within the contralateral healthy leg for comparison. The indicated noise level (dotted line) was determined from the last 5% of datapoints in time domain and is only displayed for the left-hand scale for readability.

substantiated by repeating the analysis on the  $^1\text{H}$  EG signal with high SNR (Figure S2). In this way, radial EPSI is approximately three times faster than conventional EPSI without the need for any sophisticated reconstruction techniques. More aggressive undersampling and, therefore, even stronger reduction of measurement time per 4D MRSI dataset could potentially be achieved using compressed sensing reconstructions, which has recently been applied to Cartesian-sampled EPSI.<sup>21</sup> Note that the number of necessary RF excitations for the acquisition of a single 4D MRSI dataset equals the number of required spokes. Therefore, radial undersampling might help to reduce RF saturation in dynamic experiments compared to chemical shift imaging or conventional EPSI. In this

pilot study, only a small flip angle of  $3^\circ$  was chosen to preserve the non-recoverable HP signal over a large number of spokes for demonstration purposes.

Moreover, radial sampling offers advantages in reconstruction that can be used for better modeling of the dynamics: First, the continuously repeated sampling of the k-space center enables the extraction of dynamic intra-acquisition data, resulting in a non-localized spectrum for each spoke. With this approach, all  $8 \times 60 = 480$  non-localized spectra of the in vivo measurement were quantified for the  $[1-^{13}\text{C}]$ pyruvate peak and an effective exponential  $T_{1\text{eff}}$  decay is fitted to the time course with the temporal resolution given by the repetition time (see Supporting Information S3). Second, it allows for an extraction



of subframes from a larger, fully sampled dataset, instead of using a repeating rEPSI scheme. Using techniques like keyhole<sup>22</sup> or sliding window reconstruction,<sup>23</sup> one can then not only evaluate one high resolution 4D MRSI set, but also extract dynamic information from smaller under-sampled sets, thereby increasing the temporal resolution.<sup>24</sup>

Challenges of HP <sup>13</sup>C MRSI with the proposed technique are blurring and voxel bleeding. Blurring artifacts as observed in the four-chamber phantom experiment with a long imaging duration (Figure 3) result from the T<sub>1</sub> decay affecting the intensity of each spoke, yielding an inhomogeneous distribution of the signal in k-space. Such artifacts could be compensated by either keeping the duration of spatio-spectral readouts as short as possible (as in the in vivo measurements), using variable flip angle approaches<sup>25</sup> to keep the excited signal constant during the entire acquisition, and/or using a more homogeneous sampling of consecutive spokes to spread out the signal decay more evenly across k-space.<sup>24</sup> Further, voxel bleeding arises from the broadened point spread function (PSF). Simulations revealed that the spoke sampling patterns in this study increases the real voxel size by a factor of ~1.9. For the in vivo study, this translates to an effective voxel size of 6.4 mL instead of the nominal 3.4 mL. Note that for radial readouts, B<sub>0</sub> off-resonances are another potential source of blurring: for the short readout durations of 0.5 ms (single-echo) and the typical maximal B<sub>0</sub> shifts of ~0.6 ppm in our experiments, this kind of blurring adds less than half of the voxel size to the PSF.

Although the spatiotemporal resolution is still lower than state-of-the-art imaging methods (e.g., frequency-selective EPI<sup>4</sup> or multi-echo bSSFP)<sup>26</sup> the proposed SI method is potentially useful for metabolic imaging using substrates like [1,2-<sup>13</sup>C]pyruvate or ZA at 3 T. In these cases, acquisitions with spectral resolution on the order of 10 Hz (0.3 ppm) would be desirable (e.g., enabling to resolve the spectral overlap from the doublets of [1-<sup>13</sup>C]pyruvate hydrate [upfield peak] and [1-<sup>13</sup>C]alanine [downfield peak])<sup>12</sup> or giving a pH resolution of 0.025 units in the case of ZA.<sup>10</sup> Therefore, given the typical T<sub>2</sub>\* values of these resonances in vivo of ~40 ms, aiming for a duration of spatio-spectral readouts of ~100 ms (10 Hz required spectral resolution) is plausible. To reduce the T<sub>1</sub>-filtering of k-space (T<sub>1</sub> times in vivo ~10 s) and enable dynamic series, acquisition durations of ~5 s per timeframe should be targeted, corresponding to the acquisition of only ~50 spokes. This necessitates to use alternative reconstruction strategies (e.g., keyhole or sliding window) if larger image matrices are of interest or to reduce image matrix size to ~8<sup>3</sup> for the presented setup. The most limiting factor in applying the proposed technique is gradient performance by means of achievable

physical spatial resolution at required spectral bandwidth. For dynamic imaging of [1,2-<sup>13</sup>C]pyruvate a spectral bandwidth of ~1500 Hz should be captured ideally within a single shot, limiting the spatial resolution to ~19 mm isotropic with our available gradient performance. Here, an interleaved reconstruction of odd and even echo trains could be useful instead of the summed echo train reconstruction that was used in this pilot study. This would allow to obtain the same spectral bandwidth with reduced gradient demand (i.e., 2 × 750 Hz, single-echo readout durations of 0.65 ms), which in turn would enable to increase the spatial resolution (i.e., 14 mm). This possibility is a potential benefit of a dual-echo compared to a flyback EPSI readout scheme,<sup>27</sup> besides the improved SNR efficiency using a continuous data sampling as applied in this study. Alternatively, in pH imaging with ZA where the dynamics are not of primary importance, improved spatial resolution at required spectral bandwidth could also be obtained using a multi-shot EPSI technique with spectral interleaves. However, aiming for either interleaved odd-even echo reconstruction or higher spatial resolution (i.e., denser k-space sampling), a correction for the actual gradient trajectories becomes more important than in the presented study settings.

The sequence parameters in this study were chosen mainly for demonstration purposes and are subject to further optimization in the future, as outlined above. To enable access to the proposed rEPSI sequence to the community for testing and optimization purposes, a PulSeq<sup>28</sup> implementation is provided (Supporting Information S4) offering all necessary sequence information as open-source and vendor-neutral code.

## 5 | CONCLUSION

This study demonstrated the feasibility of a 3D radial EPSI technique for HP <sup>13</sup>C MRSI in vivo. Compared to Cartesian-sampled EPSI, the radial k-space acquisition offers more aggressive acceleration capabilities with advantages like intra-acquisition T<sub>1</sub> estimation of metabolites, at the expense of a broader PSF. After optimization, the proposed method is of potential use for applications with HP <sup>13</sup>C-tracers where chemical shift information is desirable, and the acquisition of dynamic, volumetric MRSI datasets with reasonable temporal resolution is a challenge.

## ACKNOWLEDGMENTS

Research reported in this publication was supported by the German Cancer Consortium (DKTK, project HYPERBOLIC). Open Access funding enabled and organized by Projekt DEAL.

## AFFILIATIONS

<sup>1</sup>Division of Medical Physics in Radiology, German Cancer Research Center (DKFZ), Heidelberg, Germany

<sup>2</sup>Faculty of Physics and Astronomy, University of Heidelberg, Heidelberg, Germany

<sup>3</sup>Max-Planck-Institute for Nuclear Physics, Heidelberg, Germany

<sup>4</sup>Faculty of Chemistry and Earth Sciences, University of Heidelberg, Heidelberg, Germany

<sup>5</sup>German Cancer Consortium (DKTK), core center Heidelberg and German Cancer Research Center (DKFZ), Heidelberg, Germany

<sup>6</sup>Division of Medical Physics in Radiation Oncology, German Cancer Research Center (DKFZ), Heidelberg, Germany

<sup>7</sup>Department of Radiation Oncology and Radiotherapy, University Hospital Heidelberg, Heidelberg, Germany

<sup>8</sup>Heidelberg Institute for Radiation Oncology (HIRO) and National Center for Radiation Research in Oncology (NCRO), Heidelberg, Germany

<sup>9</sup>Faculty of Biosciences, University of Heidelberg, Heidelberg, Germany

<sup>10</sup>Division of Medical Physics, Department of Radiology, Medical Center, Faculty of Medicine, University of Freiburg, Freiburg, Germany

<sup>11</sup>German Cancer Consortium (DKTK), partner site Freiburg and German Cancer Research Center (DKFZ), Heidelberg, Germany

<sup>12</sup>Faculty of Medicine, University of Heidelberg, Heidelberg, Germany

## DATA AVAILABILITY STATEMENT

The code that supports the findings of this study are openly available under <http://doi.org/10.5281/zenodo.13319810>.

## ORCID

Marcel Awenius  <https://orcid.org/0009-0001-0656-6537>

Vanessa L. Franke  <https://orcid.org/0000-0002-2443-8352>

Andreas Korzowski  <https://orcid.org/0000-0002-0244-9712>

## REFERENCES

- Kurhanewicz J, Vigneron DB, Ardenkjaer-Larsen JH, et al. Hyperpolarized <sup>13</sup>C MRI: path to clinical translation in oncology. *Neoplasia*. 2019;21:1-16.
- Gordon JW, Chen HY, Dwork N, Tang S, Larson PE. Fast imaging for hyperpolarized MR metabolic imaging. *J Magn Reson Imaging*. 2021;53:686-702.
- Larson PEZ, Gordon JW. Hyperpolarized metabolic MRI—acquisition, reconstruction, and analysis methods. *Metabolites*. 2021;11:386.
- Geraghty BJ, Lau JY, Chen AP, Cunningham CH. Accelerated 3D echo-planar imaging with compressed sensing for time-resolved hyperpolarized <sup>13</sup>C studies. *Magn Reson Med*. 2017;77:538-546.
- Gordon JW, Vigneron DB, Larson PE. Development of a symmetric echo planar imaging framework for clinical translation of rapid dynamic hyperpolarized <sup>13</sup>C imaging. *Magn Reson Med*. 2017;77:826-832.
- Leupold J, Månsson S, Stefan Petersson J, Hennig J, Wieben O. Fast multiecho balanced SSFP metabolite mapping of 1 H and hyperpolarized <sup>13</sup>C compounds. *MAGMA*. 2009;22:251-256.
- Milshchey E, von Morze C, Gordon JW, Zhu Z, Larson PE, Vigneron DB. High spatiotemporal resolution bSSFP imaging of hyperpolarized [<sup>1-13</sup>C] pyruvate and [<sup>1-13</sup>C] lactate with spectral suppression of alanine and pyruvate-hydrate. *Magn Reson Med*. 2018;80:1048-1060.
- Perman WH, Bhattacharya P, Leupold J, et al. Fast volumetric spatial-spectral MR imaging of hyperpolarized <sup>13</sup>C-labeled compounds using multiple echo 3D bSSFP. *Magn Reson Imaging*. 2010;28:459-465.
- Skinner JG, Topping GJ, Nagel L, et al. Spectrally selective bSSFP using off-resonant RF excitations permits high spatiotemporal resolution 3D metabolic imaging of hyperpolarized [<sup>1-13</sup>C] pyruvate-to-[<sup>1-13</sup>C] lactate conversion. *Magn Reson Med*. 2023;90:894-909.
- Düwel S, Hundshammer C, Gersch M, et al. Imaging of pH in vivo using hyperpolarized <sup>13</sup>C-labelled zymonic acid. *Nat Commun*. 2017;8:15126.
- Grashei M, Wodtke P, Skinner JG, et al. Simultaneous magnetic resonance imaging of pH, perfusion and renal filtration using hyperpolarized <sup>13</sup>C-labelled Z-OMPD. *Nat Commun*. 2023;14:5060.
- Chen AP, Lau AZ, Yp G, Schroeder MA, Barry J, Cunningham CH. Probing the cardiac malate-aspartate shuttle non-invasively using hyperpolarized [1, 2-<sup>13</sup>C<sub>2</sub>] pyruvate. *NMR Biomed*. 2018;31:e3845.
- Cunningham CH, Chen AP, Albers MJ, et al. Double spin-echo sequence for rapid spectroscopic imaging of hyperpolarized <sup>13</sup>C. *J Magn Reson*. 2007;187:357-362.
- Eldirdiri A, Posse S, Hanson LG, et al. Development of a symmetric echo-planar spectroscopy imaging framework for hyperpolarized <sup>13</sup>C imaging in a clinical PET/MR scanner. *Tomography*. 2018;4:110-122.
- Saucedo A, Macey PM, Thomas MA. Accelerated radial echo-planar spectroscopic imaging using golden angle view-ordering and compressed-sensing reconstruction with total variation regularization. *Magn Reson Med*. 2021;86:46-61.
- Ramirez MS, Lee J, Walker CM, et al. Radial spectroscopic MRI of hyperpolarized [<sup>1-13</sup>C] pyruvate at 7 tesla. *Magn Reson Med*. 2014;72:986-995.
- Ludwig D, Korzowski A, Ruhm L, Ladd ME, Bachert P. Three-dimensional 31P radial echo-planar spectroscopic imaging in vivo at 7T. *ISMRM: Proceedings of the 25th Annual Meeting of the ISMRM*; 2017.
- O'Sullivan JD. A fast sinc function gridding algorithm for Fourier inversion in computer tomography. *IEEE Trans Med Imaging*. 1985;4:200-207.
- Korzowski A, Weinfurter N, Mueller S, et al. Volumetric mapping of intra- and extracellular pH in the human brain using 31P MRSI at 7T. *Magn Reson Med*. 2020;84:1707-1723.
- Vanhamme L, van den Boogaart A, Van Huffel S. Improved method for accurate and efficient quantification of MRS data with use of prior knowledge. *J Magn Reson*. 1997;129:35-43.
- Chen HY, Larson PE, Gordon JW, et al. Technique development of 3D dynamic CS-EPSI for hyperpolarized <sup>13</sup>C pyruvate MR molecular imaging of human prostate cancer. *Magn Reson Med*. 2018;80:2062-2072.
- Morik H-A, Schuenke P, Schröder L. Rapid analytical CEST spectroscopy of competitive host-guest interactions using spatial parallelization with a combined approach of variable flip

- angle, keyhole and averaging (CAVKA). *Phys Chem Chem Phys*. 2022;24:12126-12135.
23. d'Arcy J, Collins D, Rowland I, Padhani A, Leach M. Applications of sliding window reconstruction with cartesian sampling for dynamic contrast enhanced MRI. *NMR Biomed*. 2002;15:174-183.
  24. Rincon G, Awenius M, Abeln H, et al. GAGA: gapped arrangement of Golden angles for sliding window reconstruction of hyperpolarized dynamic  $^{13}\text{C}$  MRSI data acquired with 3D radial EPSI. *ESMI: Proceedings of the 19th Annual Meeting of the EMIM*; 2024.
  25. Xing Y, Reed GD, Pauly JM, Kerr AB, Larson PE. Optimal variable flip angle schemes for dynamic acquisition of exchanging hyperpolarized substrates. *J Magn Reson*. 2013;234:75-81.
  26. Müller CA, Hundshammer C, Braeuer M, et al. Dynamic 2D and 3D mapping of hyperpolarized pyruvate to lactate conversion in vivo with efficient multi-echo balanced steady-state free precession at 3 T. *NMR Biomed*. 2020;33:e4291.
  27. Santos-Díaz A, Obruchkov SI, Schulte RF, Noseworthy MD. Phosphorus magnetic resonance spectroscopic imaging using flyback echo planar readout trajectories. *MAGMA*. 2018;31:553-564.
  28. Layton KJ, Kroboth S, Jia F, et al. Pulseseq: a rapid and hardware-independent pulse sequence prototyping framework. *Magn Reson Med*. 2017;77:1544-1552.

## SUPPORTING INFORMATION

Additional supporting information may be found in the online version of the article at the publisher's website.

### Data S1. Supporting information.

**How to cite this article:** Awenius M, Abeln H, Müller M, et al. Three-dimensional radial echo-planar spectroscopic imaging for hyperpolarized  $^{13}\text{C}$  MRSI in vivo. *Magn Reson Med*. 2025;93:31-41. doi: 10.1002/mrm.30258